

QPSO-ILF-ANN-based optimization of TBM control parameters considering tunneling energy efficiency

Xinyu WANG^{a,b}, Jian WU^{b,c}, Xin YIN^{b*}, Quansheng LIU^b, Xing HUANG^d, Yucong PAN^b, Jihua YANG^a, Lei HUANG^c, Shuangping MIAO^c

^a Yellow River Engineering Consulting Co., Ltd., Zhengzhou 450003, China

^b School of Civil Engineering, Wuhan University, Wuhan 430072, China

^c Power China Huadong Engineering Co., Ltd., Hangzhou 311122, China

^d State Key Laboratory of Geomechanics and Geotechnical Engineering, Institute of Rock and Soil Mechanics, Chinese Academy of Sciences, Wuhan 430071, China

*Corresponding author. E-mail: yinxin_engineering@163.com

© Higher Education Press 2023

ABSTRACT In recent years, tunnel boring machines (TBMs) have been widely used in tunnel construction. However, the TBM control parameters set based on operator experience may not necessarily be suitable for certain geological conditions. Hence, a method to optimize TBM control parameters using an improved loss function-based artificial neural network (ILF-ANN) combined with quantum particle swarm optimization (QPSO) is proposed herein. The purpose of this method is to improve the TBM performance by optimizing the penetration and cutterhead rotation speeds. Inspired by the regularization technique, a custom artificial neural network (ANN) loss function based on the penetration rate and rock-breaking specific energy as TBM performance indicators is developed in the form of a penalty function to adjust the output of the network. In addition, to overcome the disadvantage of classical error backpropagation ANNs, i.e., the ease of falling into a local optimum, QPSO is adopted to train the ANN hyperparameters (weight and bias). Rock mass classes and tunneling parameters obtained in real time are used as the input of the QPSO-ILF-ANN, whereas the cutterhead rotation speed and penetration are specified as the output. The proposed method is validated using construction data from the Songhua River water conveyance tunnel project. Results show that, compared with the TBM operator and QPSO-ANN, the QPSO-ILF-ANN effectively increases the TBM penetration rate by 14.85% and 13.71%, respectively, and reduces the rock-breaking specific energy by 9.41% and 9.18%, respectively.

KEYWORDS tunnel boring machine, control parameter optimization, quantum particle swarm optimization, artificial neural network, tunneling energy efficiency

1 Introduction

During the construction of tunnel boring machines (TBMs), the selection and adjustment of the control parameters affect the tunneling performance and construction efficiency. Currently, TBM control parameters are adjusted primarily based on operator experience, which is not a highly accurate method. The operational errors of the TBM driver can result in a severely worn

cutterhead in certain cases, which consequently affects the excavation speed [1]. Hence, control parameters should be specified based on the current geological conditions and driving parameters to ensure safe and efficient TBM construction.

Recently, several TBM construction and control parameter prediction methods have been proposed. Hasanpour et al. [2] investigated the effects of different geological and machine parameters on the thrust required for a single-shield TBM in a squeezing stratum and proposed a TBM thrust prediction model. Shirlaw et al. [3] analyzed

the relationship among the rock-breaking specific energy, field penetration index (*FPI*), and ring number, which provides a basis for adjusting the TBM mud cycling process. By performing simulations and on-site excavation tests, Ramoni and Anagnostou [4] and Zhao et al. [5] predicted the thrust required for TBMs. Huo et al. [6] analyzed the effect of the cutterhead rotation speed on its vibration, and the results showed that the appropriate cutterhead rotation speed must be selected to avoid accidents such as bearing damage and seal failure.

Owing to advances in computer technology, many artificial intelligence methods have been proposed for solving complex engineering problems [7–9]. Artificial intelligence algorithms typically perform better than classical regression methods [10]. Wang et al. [11] proposed a comprehensive prediction model based on TBM operation data and geological information using four machine learning algorithms to assist in TBM operations. To predict the TBM parameters in real time, a long short-term memory (LSTM) neuron network was used [12]. Gao et al. [13] proposed a real-time method for predicting TBM operating parameters in which a recurrent neural network, LSTM, and gated recurrent unit network were used to predict the TBM operating parameters. Moreover, LSTM was combined with a one-dimensional convolutional neural network (CNN) to develop a TBM cutterhead rotation speed and penetration prediction model [14]. Guo et al. [15] proposed a TBM assistant driving method that applies deep learning to determine the appropriate thrust and cutterhead torque based on the integrity of the surrounding rock. Additionally, the Monte Carlo-backpropagation (BP) neural network [16], the fuzzy logic method [17], extreme gradient boosting [18], and the transformed temporal pattern (TransTP) network [19] were used to develop models for predicting TBM parameters. Compared with classical statistical regression methods, models based on machine learning algorithms typically afford better prediction performance [20].

As the TBM cutterhead system is extremely sensitive to geological conditions, the TBM control parameters must be appropriately adjusted during excavation to obtain the best tunneling performance under certain geological conditions. Many indicators can reflect TBM performance, such as the cutterhead thrust (*T*), *FPI*, rock-breaking specific energy (E_s), advance rate, and penetration rate (*V*). Many models for estimating these indicators have been developed [21–23]. Meanwhile, some researchers have proposed an optimization method for control parameters based on tunneling performance. Yang et al. [24] established an optimal control strategy for the cutterhead system mode using the prediction results of the cutterhead load and efficiency to control the energy consumption. Xue et al. [25] proposed a method for selecting TBM control parameters based on the principle

of optimal energy. Liu et al. [26] proposed an intelligent decision-making method based on multi-objective optimization that considers mining efficiency and cost. Gong et al. [27] developed a real-time analysis system based on machine vision and deep learning and then applied it to optimize TBM operation parameters. Xia et al. [28] improved the residue performance of TBMs by optimizing the penetration and cutterhead speeds. In general, TBM energy consumption and efficiency are the main indicators of tunneling performance. However, most classical models trained on historical data rely on driver experience. Under certain geological conditions, the optimized penetration and cutterhead rotation speeds should increase the penetration rate of the TBM and reduce the E_s such that it is lower than empirical values.

The aim of the current study is to develop a method that optimizes the TBM penetration and cutterhead rotation speeds to increase the tunnel excavation speed and reduce the rock-breaking energy consumption. Hence, a hybrid algorithm that combines quantum particle swarm optimization (QPSO) and an improved-loss function-based artificial neural network (ILF-ANN), denoted as QPSO-ILF-ANN, is proposed herein. The cutterhead rotation speed and penetration optimization are estimated by improving the loss function of the ANN. In addition, QPSO is used to replace the gradient descent method, which is typically utilized during the training of classical ANN models. The optimization results of the model can provide a basis for specifying TBM control parameters.

2 Methodology

2.1 Artificial neural network

ANNs are a widely used machine learning technique for solving regression and classification problems. They typically comprise input, hidden, and output layers [29,30]. Figure 1 illustrates a typical three-layer ANN topology.

The connection weight and bias are the most important hyperparameters of an ANN. These parameters are optimized during the training of the ANN via an error BP

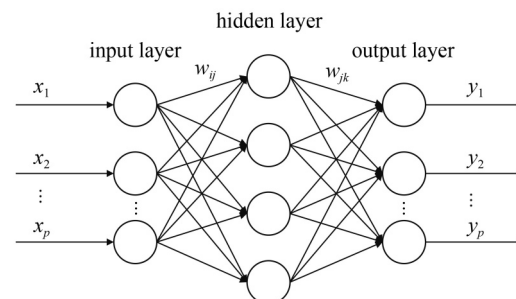


Fig. 1 Typical three-layer ANN.

approach that minimizes the loss function [31]. The loss function of an ANN is typically defined as

$$Loss = \frac{1}{m} \sum_{k=1}^m (y^k - \hat{y}^k)^2, \quad (1)$$

where m is the total number of training samples; y^k and \hat{y}^k are the actual and predicted values of the k th training dataset, respectively.

2.2 Quantum particle swarm optimization

Particle swarm optimization (PSO) is a heuristic swarm intelligence algorithm that simulates the predatory behavior of birds via information sharing to transform disordered particles to ordered ones such that the optimal solution can be obtained in a search space [32,33]. Inspired by quantum science, quantum particle swarm optimization (QPSO) is an improved version of the PSO that overcomes the premature problem [34].

Generally, QPSO assumes that the particles in a population exhibit quantum behavior. Each particle propagates in a P -centered δ -potential well where its position and velocity cannot be determined simultaneously. Hence, a Monte Carlo stochastic simulation is introduced to update the particle positions. The position of the i th particle at the $(t + 1)$ th iteration can be calculated as follows.

$$x_i(t+1) = \theta \cdot pbest_i + (1 - \theta) \cdot gbest \pm \frac{L(t)}{2} \cdot \ln \frac{1}{u}, \quad (2)$$

where θ and u are random numbers between 0 and 1, $pbest_i$ is the optimal position searched by the i th particle, $gbest$ is the optimal position searched by all particles, and $L(t)$ is the characteristic length of the δ -potential well.

2.3 Artificial neural network combined with quantum particle swarm optimization

The classical training process of ANNs with error BP presents a few disadvantages, including gradient disappearance and falling into a local optimum [35,36]. Thus, to improve the capabilities of the ANN model, QPSO is combined with an ANN to develop an optimized model for control parameters. In particular, QPSO particles are introduced at the connection weights and biases of the ANN. Accordingly, the loss function of the ANN is minimized, whereas the ANN weights and biases are adjusted via QPSO instead of error BP, as shown in Fig. 2.

3 Database description

3.1 Project overview

The database used in this research was obtained from the

TBM3 section of the Songhua River water conveyance tunnel project, built in Jilin Province, China. The total length of the study area was 11.2 km (i.e., (56 + 700) to (67 + 900) m), with a maximum buried depth of 260 m. In this study, the surrounding rock was classified into four classes based on the code for the geological engineering investigation of water resources and hydropower (GB50287-2008) [37]. Figure 3 shows the percentages of classes II, III, IV, and V, i.e., 11.81%, 61.45%, 15.57%, and 11.17%, respectively. Figure 4 shows the geological profile of the study area, which is primarily comprised of tuff, diorite, granite, sandstone, and limestone. An open-type TBM was adopted for the construction, and the main technical parameters are listed in Table 1.

3.2 Database establishment

The TBM's operating data included those from shutdown and driving stages. Based on the data change trend, the driving stage can be classified as idle, rising, or steady [38]. To account for the rock-TBM interaction during modeling, one must eliminate the shutdown and idle

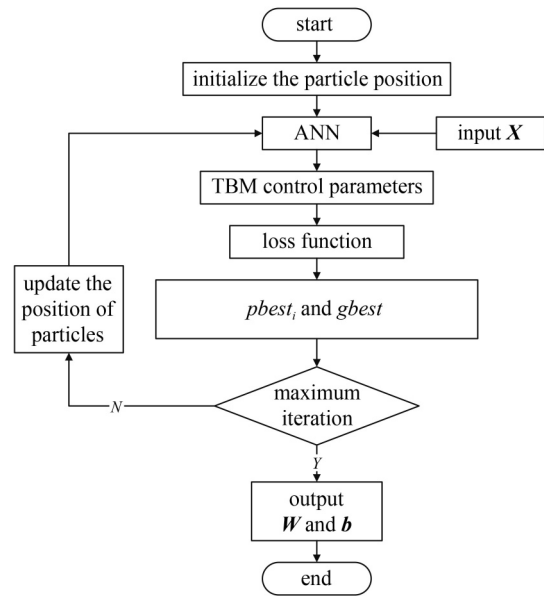


Fig. 2 QPSO-ANN framework.

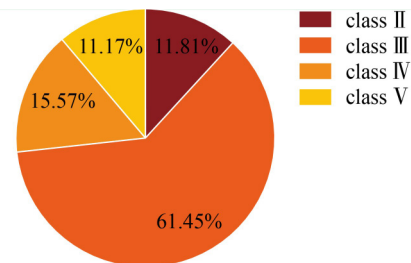


Fig. 3 Proportion of rock mass classes.

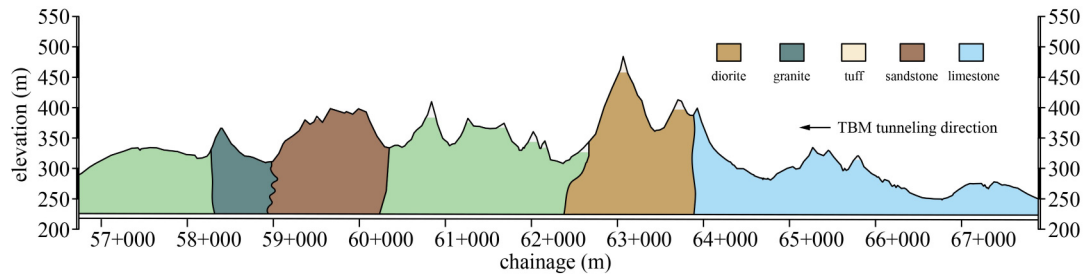


Fig. 4 Geological profile of study area.

Table 1 Main specifications of the TBM

technical parameter	design value
cutterhead diameter (mm)	7930
number of hobs	56
cutterhead distance (mm)	70–89
rated thrust (kN)	23260
propulsion cylinder stroke (mm)	1800
rated torque (kN·m)	8410
maximum cutterhead speed ($r \cdot \min^{-1}$)	7.6

stages of the database. Accordingly, the binary discriminant function defined in Eqs. (3)–(5) is used to identify the shutdown and driving stages.

$$S = f(F) \cdot f(T) \cdot f(RPM) \cdot f(PRev), \quad (3)$$

$$f(x) = \begin{cases} 1, & x \neq 0, \\ 0, & x = 0, \end{cases} \quad (4)$$

$$S = \begin{cases} 1, & \text{driving,} \\ 0, & \text{shutdown,} \end{cases} \quad (5)$$

where F is the cutterhead thrust, T the cutterhead torque, RPM the cutterhead rotation speed, and $PRev$ the TBM penetration.

After eliminating the shutdown-stage data, the idle-stage data must be identified and removed. Hou and Liu [39] analyzed on-site TBM data and discovered that when a TBM established contact with the surrounding rocks from an idle state, the driving parameters declined significantly prior to the rising stage, and the duration of the idle stage was generally less than 60 s. Therefore, the time corresponding to the peak value in the first 60 s of the idle stage can be regarded as the time at which the cutterhead establishes contact with the surrounding rock. Hence, the minimum value in the range of $[t, t + 30]$ was used as the starting time of the rising stage. Accordingly, the method above was used in this study to identify the breaking point of the idle and rising stages and to extract data from the first 30 s of the rising stage. Comparative assessments of field data showed that the total duration of the idle and rising stages in a cyclic excavation process

did not exceed 200 s [37]. Hence, the 300th second of the driving stage were used in this study as the starting moment of the steady stage. The data for each driving parameter in the first 600 s of the steady stage were extracted as their representative values. The classification of the TBM driving parameters is shown in Fig. 5. After processing, a TBM driving parameter dataset containing 4459 excavation cycles was obtained. Each excavation cycle comprised 30 s of rising-stage data and 600 s of steady-stage data.

The processed parameters can be matched with geological data using chainage information. Accordingly, the database contains 4459 excavation cycles, including the TBM driving parameters and the corresponding rock mass classes. Generally, the driving parameters include those of the main driving and cutterhead systems, such as thrust, cutterhead torque, penetration rate, cutterhead rotation speed, and penetration. In addition, the rock mass classes were classes II, III, IV, and V (the HC method).

4 Model establishment

4.1 Selection of input features

In an excavation cycle, the changes in the driving parameters of each rising stage are reflected in the geological conditions under certain control parameters. Therefore, the driving parameters of the rising stage were adopted in this study as the input argument to predict the control parameters of the steady stage.

Based on an analysis of previous studies [13,40–42], the following input parameters were used in this study: cutterhead torque, cutterhead thrust, cutterhead power, penetration, and excavation rate. The cutterhead torque reflects the hardness and integrity of a rock mass. The cutterhead thrust is primarily affected by the uniaxial compressive strength of the rock. The cutterhead power can be regarded as the combined effect of the cutterhead torque and cutterhead thrust. The penetration depth indicates the depth of cut in one revolution of the cutterhead, and the penetration rate represents the distance traversed by the TBM per unit of time. The penetration depth and rate are important indicators for measuring the excavatability of a rock mass. The

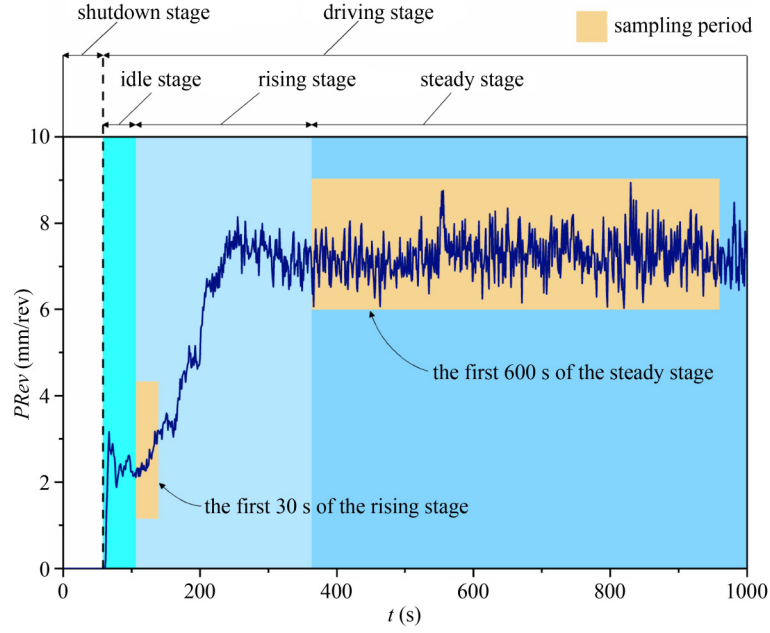


Fig. 5 Classification of TBM driving parameters.

least-squares method was used to obtain a fitting line for each of the parameters above (X_i) in the rising stage, as shown in Fig. 6. Subsequently, the slope of the fitting line (X_i^k), root mean squared error of the fitting line (X_i^R), and mean value of X_i (X_i^m) were used as inputs for the model. In addition, the rock mass class was used as the input. Sixteen features were selected as inputs for the model, and the output of the model included two parameters, as shown in Eqs. (6) to (8). Moreover, X^R can be calculated using Eq. (9).

$$\mathbf{X} = [X_1, X_2, X_3, X_4, X_5, R_c], \quad (6)$$

$$X_i = [X_i^m, X_i^k, X_i^R], \quad (7)$$

$$\mathbf{Y} = [PRev, RPM], \quad (8)$$

$$X^R = \sqrt{\frac{\sum_{t=1}^T (X(t) - f_X(t))^2}{T}}, \quad (9)$$

where \mathbf{X} and \mathbf{Y} are the input and output vectors of the model, respectively; X_1 to X_5 are the vectors of the cutterhead thrust, cutterhead torque, cutterhead power, penetration, and penetration rate, respectively; R_c is the rock mass class; X_i^m , X_i^k , and X_i^R are the mean, slope, and volatility of parameter X_i , respectively; $PRev$ and RPM are the penetration depth and cutterhead rotation speeds, respectively; $f_X(t)$ is the fitting line of X in the rising stage; T is the length of the stage interval, which was set as 30 s in this study.

As the rock mass classes were discrete variables and their hierarchical results exhibited an inner-order

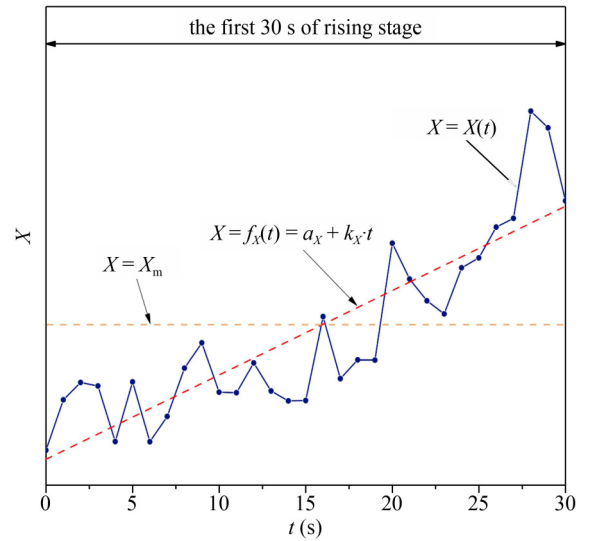


Fig. 6 Fitting line of driving parameter X in rising stage.

relationship, rock mass classes II–V were mapped to integers 1–4, respectively. The output parameters of the model were regarded as the mean values of RPM and $PRev$ in the steady stage.

4.2 Improved loss function-based artificial neural network combined with quantum particle swarm optimization

In on-site engineering, the selection and adjustment of TBM control parameters primarily depends on operator experience. In fact, most of the settings specified cannot yield the optimum tunneling performance under specific geological conditions. Therefore, the values of RPM and $PRev$ must be optimized based on model prediction

results. In this study, the penetration rate was selected to characterize the TBM tunneling performance and was specified as the optimization goal of the aided decision-making model.

The penetration rate (V) is one of the main factors that determines the construction efficiency of TBMs. It is defined as the distance of the TBM excavating forward within a unit of time and is calculated as follows:

$$V = RPM \cdot PRev. \quad (10)$$

Crack propagation and rock fragmentation are complex physical processes [43,44]. The rock-breaking specific energy (E_s) is defined as the energy consumed by the cutterhead to cut a unit volume of rock blocks [45]. Typically, it is used to characterize the rock-breaking energy consumption of a TBM cutterhead and is calculated as follows [46].

$$E_s = \frac{F \cdot PRev + 2\pi T}{\pi R^2 \cdot PRev}, \quad (11)$$

where F is the cutterhead thrust (kN), T the cutterhead torque (kN·m), and R the cutterhead radius (m).

The lower the E_s , the higher is the rock-breaking efficiency. To optimize E_s and V , a QPSO-ILF-ANN model was developed in this study by improving the loss function of the QPSO-ANN. The improved loss function is defined as follows.

$$Loss' = Loss + E_s + (-V), \quad (12)$$

where E_s and V are the rock-breaking specific energy and penetration rate, respectively, obtained via the current control-parameter calculation.

E_s and V in Eq. (12) are used to penalize the loss functions, and their values are affected by the control parameters. During model training, the calculated value of $Loss'$ provides important feedback for adjusting the output values of the control parameters.

4.3 Calculation of loss function

Equation (12) comprises three terms, among which $Loss$ and V can be calculated using Eqs. (1) and (10), respectively. However, E_s cannot be calculated using Eq. (11) because the relationship among F , T , and the control parameters is unknown. Zhang et al. [47] proposed a formula for predicting E_s via regression analysis; however, the foundation capacity required for the formula is difficult to obtain during TBM construction. Because F and T depend on the geological conditions and control parameters, and the geological conditions can be reflected by the driving data characteristics of the rising stage and rock mass class, an E_s prediction model can be developed. In particular, the model inputs are the driving parameters of the rising stage, the rock mass class, and the control parameters of the steady stage. The

calculation of the driving parameters in the rising stage is presented in Subsection 4.1. The model output is E_s under specific control parameters and geological conditions.

In this study, the random forest (RF) machine learning technique [48] was used to develop an E_s prediction model. Generally, in the RF method, bagging is adopted to ensemble decision trees, and random attribute selection is applied to the node-partitioning process. Compared with classical decision trees, the RF reduces the risk of overfitting and improves the generalization ability of a model. RF has been widely used in many practical tasks and has demonstrated excellent performance [49]. A more detailed introduction to RF is presented in Ref. [50]. Prior to training the machine learning model, the sample data were normalized using Eq. (13).

$$x_{\text{norm}} = \frac{x - x_{\min}}{x_{\max} - x_{\min}}, \quad (13)$$

where x and x_{norm} represent the feature variables before and after normalization, respectively; x_{\min} and x_{\max} represent the minimum and maximum values of the feature variables in the sample, respectively.

The 4459 samples were classified into 4013 training samples (90%) and 446 test samples (10%), and the actual E_s value was calculated using Eq. (11). The RF hyperparameters were optimized via grid search with 10-fold cross-validation [51]. The optimization process is illustrated in Fig. 7. Table 2 shows the hyperparameter ranges of the RF model, where T_c represents the number of decision trees contained in the RF, minLF the minimum number of leaf node samples on the tree, and maxDP the maximum depth of the tree. Each possible hyperparameter combination was traversed via grid search, and the optimal hyperparameters were determined based on 10-fold cross-validation results.

The results of the hyperparameter optimization are shown in Fig. 8. The RF model achieved the best prediction performance when T_c , minLF , and maxDP were 400, 1, and 42, respectively. The results predicted by the RF model for the test samples are shown in Fig. 9. As shown, the RF model predicted E_s accurately, with an R^2 of 0.905. Therefore, the RF model is suitable for evaluating E_s under specific geological conditions and control parameters.

The training process of the QPSO-ILF-ANN is illustrated in Fig. 10. In general, E_s is predicted in the current iteration after the model outputs the RPM and $PREV$. Subsequently, the improved loss function $Loss'$ is calculated and used as the fitness function for the next iteration of the model.

5 Model prediction results

The main hyperparameters of the QPSO-ILF-ANN

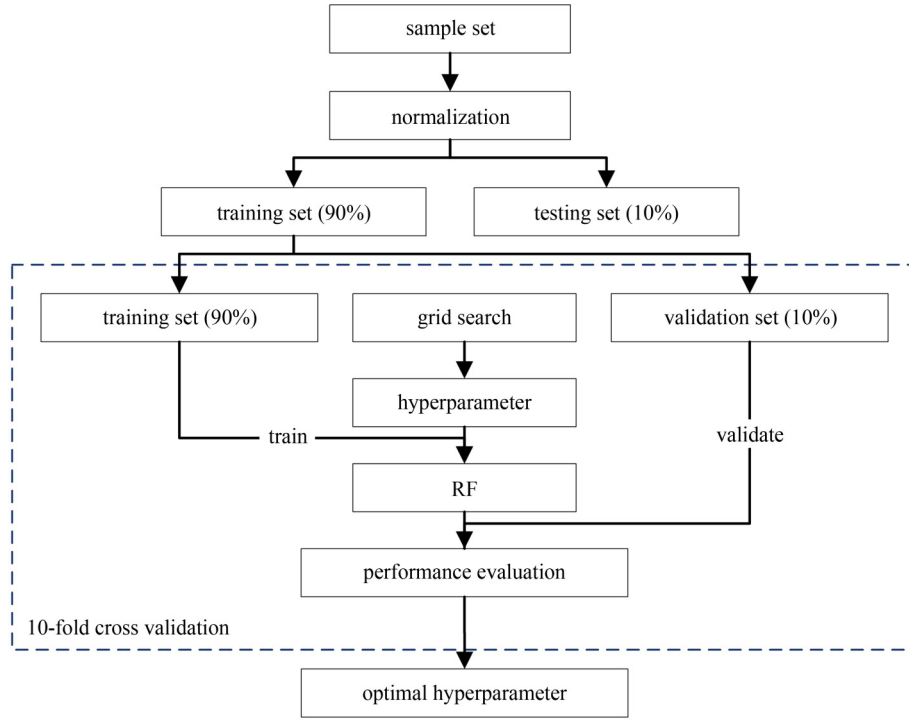


Fig. 7 Hyperparameter optimization process.

include the population size (POP), contraction and expansion factor (β), hidden layer number of the neural network ($nLayer$), and number of neurons in the hidden layer ($nNeure$). Both POP and β primarily affect the search range and convergence speed of the QPSO algorithm. Meanwhile, $nLayer$ and $nNeure$ primarily affect the prediction accuracy of the model. The hyperparameters of the model were optimized using grid search and 10-fold cross-validation. The prediction results of the model were evaluated using the mean absolute percent error ($MAPE$), which is calculated as follows.

$$MAPE = \frac{1}{m} \sum_{i=1}^m \left| \frac{y_i - \hat{y}_i}{y_i} \right| \times 100\%, \quad (14)$$

where y_i is the measured value of sample i , \hat{y}_i the

Table 2 Hyperparameter ranges of RF model used in current study

hyperparameter	range of value
T_c	2, 5, 10, 50, 100, 150, 200, 250, 300, 400
$minLF$	[1,10]
$maxDP$	[2,50]

predicted value of sample i , and m the number of samples in the test set.

The lower the $MAPE$, the better the performance of the model. The range of values and the optimization results for each hyperparameter are listed in Table 3.

The output results of the QPSO-ILF-ANN model for 446 test samples are shown in Figs. 11(a)–11(d). Figures 12(a) to 12(d) show the optimization effects of the model on E_s and V . In general, the control parameters provided by QPSO-ILF-ANN in most samples achieved

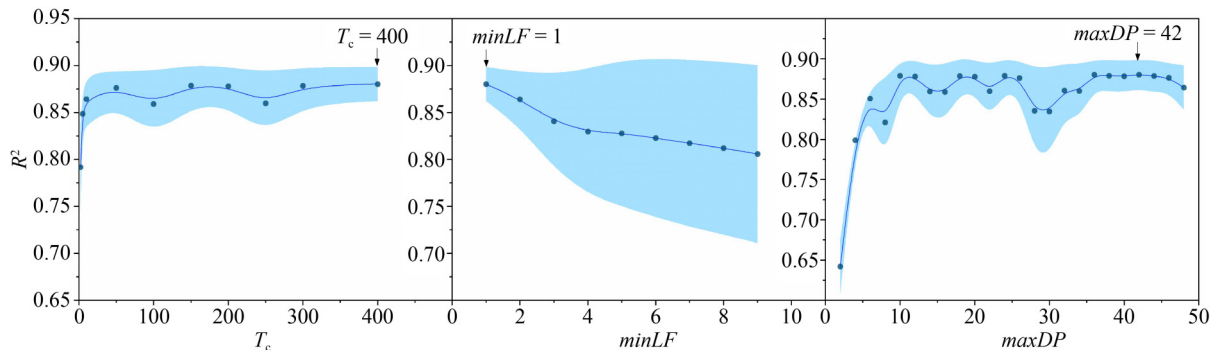


Fig. 8 RF model hyperparameter optimization results.

lower E_s and higher V values as compared with those provided by the QPSO-ANN model and the operator. The output effects of the QPSO-ILF-ANN and QPSO-ANN models on E_s and V are summarized in Fig. 13. The mean values of E_s and V obtained by the QPSO-ANN model for the test samples were 7.95 MJ/m^3 and 65.51 mm/min , respectively, and those of the QPSO-ILF-ANN were 7.22 MJ/m^3 and 74.49 mm/min , respectively. Moreover, optimizing the control parameters in the QPSO-ILF-ANN model reduced E_s by 9.18% and increased V by an average of 13.71% as compared with the performance of the QPSO-ANN model. Additionally, the QPSO-ILF-ANN model reduced E_s by 9.41% and increased V by 14.85% as compared with the performance based on driver experience ($E_s = 7.97 \text{ MJ/m}^3$, $V = 64.86 \text{ mm/min}$).

6 Conclusions

Instead of being set based on precise geological conditions, the values of TBM control parameters are often estimated based on driver experience. A method for optimizing TBM control parameters based on the penetration rate and rock-breaking specific energy was proposed herein. The approach was developed using a hybrid model that combined QPSO and an ILF-ANN. Sixteen features, including tunneling parameters and rock mass classes, were used as inputs to the model. In

addition, the control parameters, including the cutterhead rotation speed and penetration, were used as outputs. The penetration rate and rock-breaking specific energy were added to the loss function of the ILF-ANN in the form of dependent variables for the cutterhead rotation speed and penetration to adjust the model output automatically. A QPSO was performed to train the neural network parameters and improve the global optimization performance of the model. Finally, the model was validated using field data obtained from the Songhua River water conveyance tunnel project. The results showed that the proposed method achieved effective optimization performance. Compared with the cutterhead rotation speeds and penetration outputs of the TBM operator and QPSO-ANN, those of the QPSO-ILF-ANN increased the penetration rate by 14.85% and 13.71%, respectively, and reduced the rock-breaking specific energy by 9.41% and 9.18%, respectively. The various weights of the penetration rate and the rock-breaking specific energy in the loss function of the ANN were not considered in this study. Under different geological conditions, the effects of efficiency and energy consumption on TBM performance are typically different. In the future, the effects of the weights of the

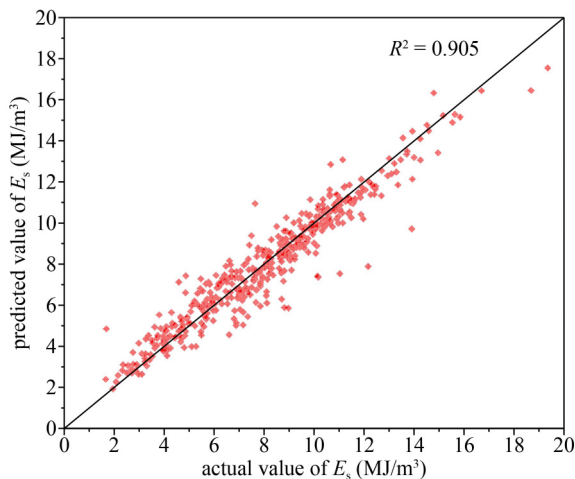


Fig. 9 RF model prediction results.

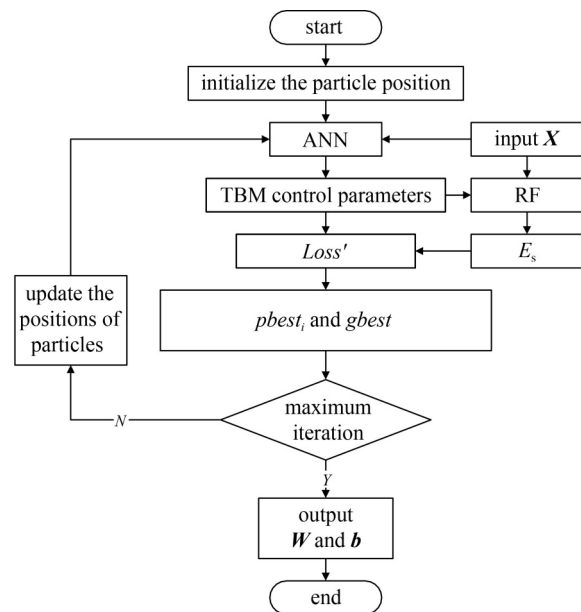


Fig. 10 QPSO-ILF-ANN algorithm framework.

Table 3 QPSO-ILF-ANN model hyperparameter optimization results

hyperparameter	range of value	optimization result
POP	50, 100, 200, 400, 600, 800, 1000	600
β	[0.1, 0.5], [0.2, 0.5], [0.3, 0.5], [0.5, 0.7], [0.5, 0.8], [0.5, 0.9], [0.3, 0.7], [0.2, 0.8], [0.1, 0.9]	[0.3, 0.7]
nLayer	1, 2	2
nNeure	[2 ³ , 2 ⁶]	(32,16)

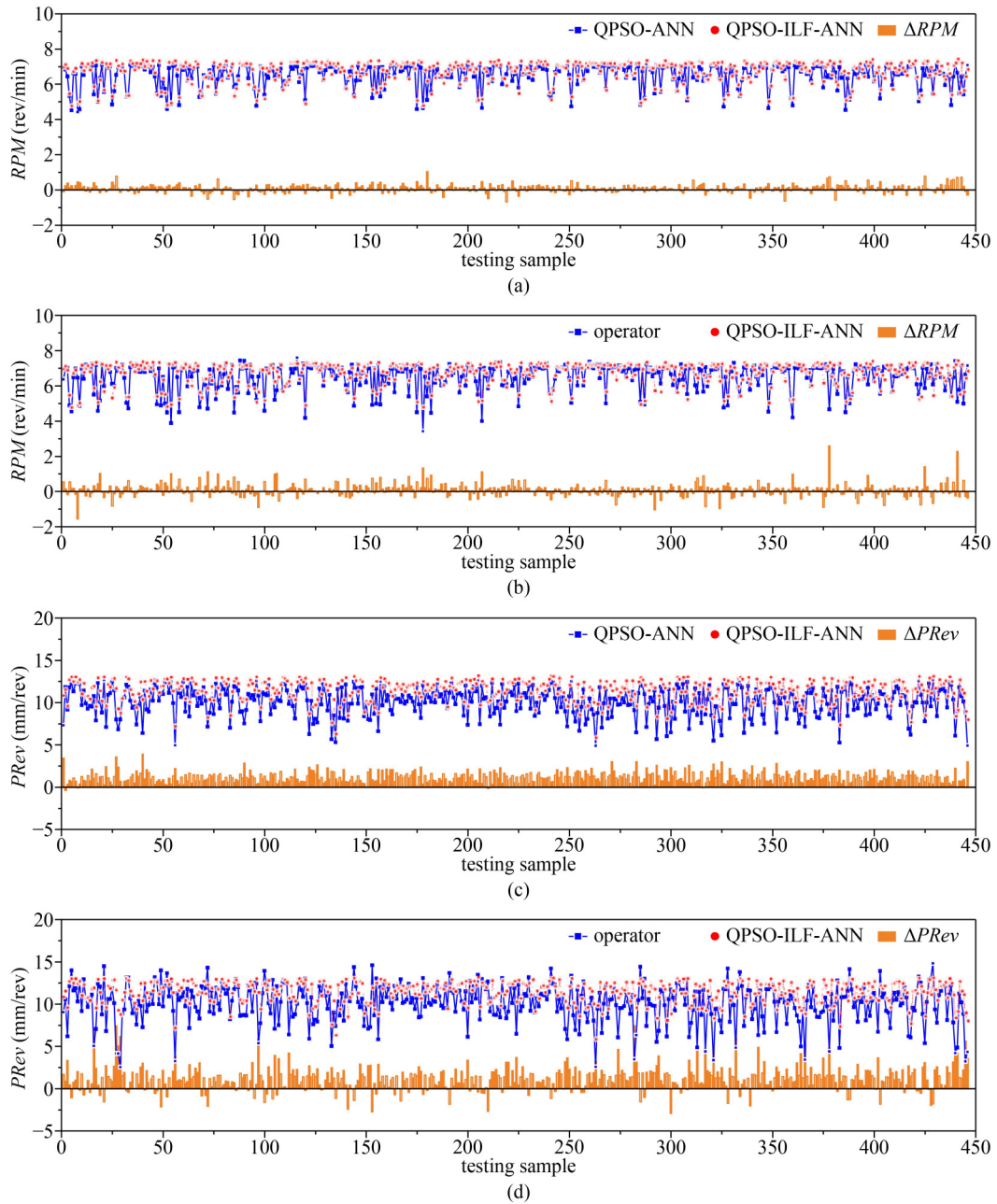
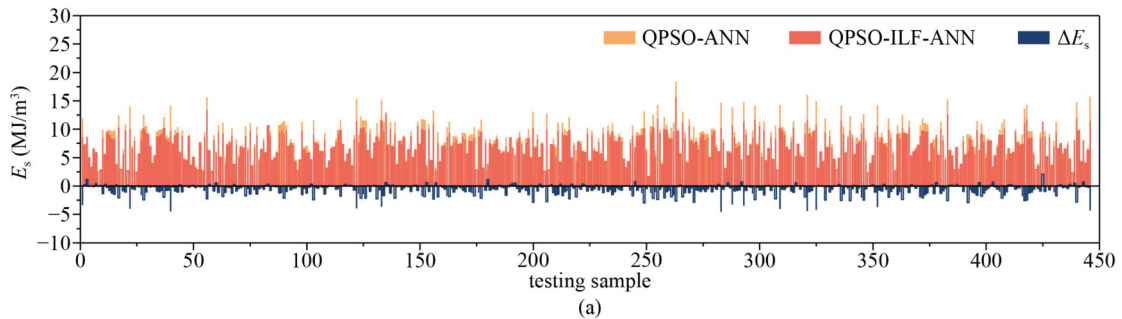


Fig. 11 Model output results: (a) RPM : QPSO-ILF-ANN vs. QPSO-ANN; (b) RPM : QPSO-ILF-ANN vs. operator's operation; (c) $PRev$: QPSO-ILF-ANN vs. QPSO-ANN (d) $PRev$: QPSO-ILF-ANN vs. operator's operation.



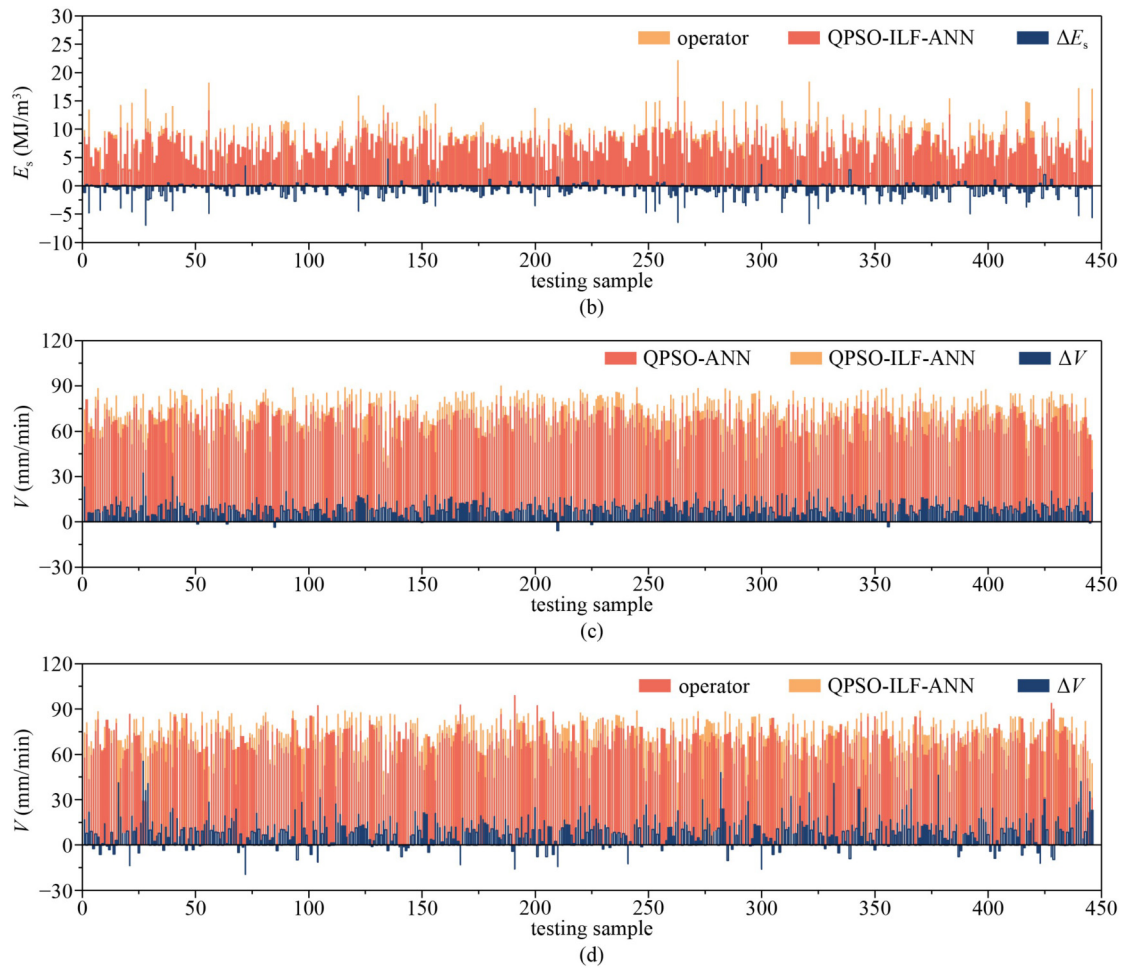


Fig. 12 Optimization results of rock-breaking specific energy and penetration rate: (a) E_s : QPSO-ILF-ANN vs. QPSO-ANN; (b) E_s : QPSO-ILF-ANN vs. operator’s operation; (c) V : QPSO-ILF-ANN vs. QPSO-ANN; (d) V : QPSO-ILF-ANN vs. operator’s operation.

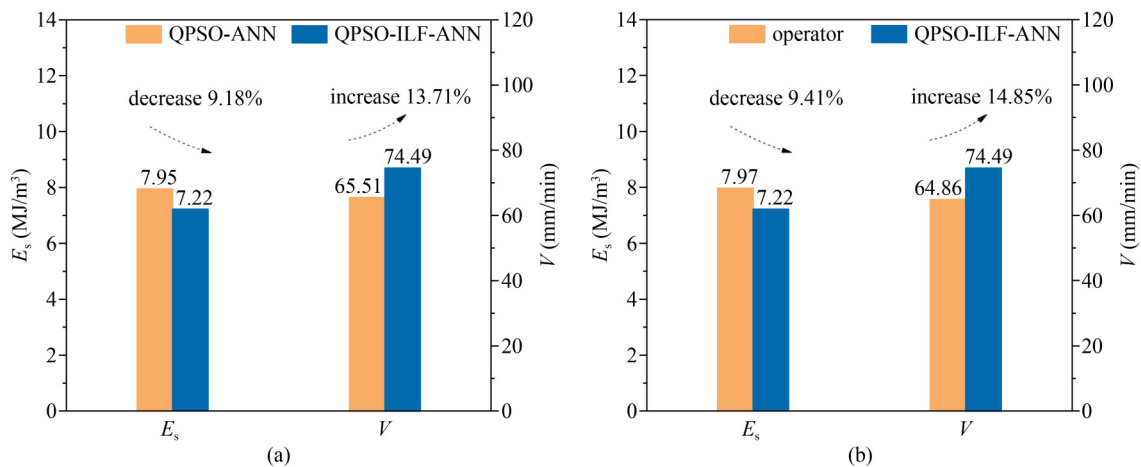


Fig. 13 Optimization results of rock-breaking specific energy and penetration rate. (a) QPSO-ANN and QPSO-ILF-ANN; (b) operator’s operation and QPSO-ILF-ANN.

penetration rate and rock-breaking specific energy will be considered in the development of TBM tunneling modes for different geological conditions.

Acknowledgements This study was supported by the National Natural Science Foundation of China (Grant Nos. 41941018, 52074258, 42177140, and 41807250), and the Key Research and Development Project of Hubei

Province (No. 2021BCA133). We gratefully acknowledge the support provided.

References

- Liu B, Chen L, Wang R R, Wang Y X. Research progress and prospect of adverse geology forward-prospecting and intelligent decision-making of TBM tunneling. In: Proceedings of Sixth International Conference on Engineering Geophysics. Tulsa: Society of Exploration Geophysicists, 2021, 134–138
- Hasanpour R, Rostami J, Thewes M, Schmitt J. Parametric study of the impacts of various geological and machine parameters on thrust force requirements for operating a single shield TBM in squeezing ground. *Tunnelling and Underground Space Technology*, 2018, 73: 252–260
- Shirlaw J N, Henderson T O, Haryono I S, Dudouit F, Salisbury D. The effect of altering the slurry circulation system on TBM tunnelling in weathered Kowloon granite. *Tunnelling and Underground Space Technology*, 2022, 124: 104474
- Ramoni M, Anagnostou G. Thrust force requirements for TBMs in squeezing ground. *Tunnelling and Underground Space Technology*, 2010, 25(4): 433–455
- Zhao K, Janutolo M, Barla G. A completely 3D model for the simulation of mechanized tunnel excavation. *Rock Mechanics and Rock Engineering*, 2012, 45(4): 475–497
- Huo J Z, Wu H Y, Yang J, Sun W, Li G Q, Sun X L. Multi-directional coupling dynamic characteristics analysis of TBM cutterhead system based on tunnelling field test. *Journal of Mechanical Science and Technology*, 2015, 29(8): 3043–3058
- Tiachacht S, Bouazzouni A, Khatir S, Abdel Wahab M, Behtani A, Capozucca R. Damage assessment in structures using combination of a modified Cornwell indicator and genetic algorithm. *Engineering Structures*, 2018, 177: 421–430
- Dsouza S M, Varghese T M, Budarapu P R, Natarajan S. A non-intrusive stochastic isogeometric analysis of functionally graded plates with material uncertainty. *Axioms*, 2020, 9(3): 92
- Varma V S, Yogeshwar Rao R, Vundavilli P R, Pandit M K, Budarapu P R. A machine learning-based approach for the design of lower limb exoskeleton. *International Journal of Computational Methods*, 2022, 19(8): 2142012
- Cuong-Le T, Minh H L, Khatir S, Wahab M A, Tran M T, Mirjalili S. A novel version of Cuckoo search algorithm for solving optimization problems. *Expert Systems with Applications*, 2021, 186: 115669
- Wang X, Zhu H H, Zhu M Q, Zhang L Y, Ju J W. An integrated parameter prediction framework for intelligent TBM excavation in hard rock. *Tunnelling and Underground Space Technology*, 2021, 118: 104196
- Gao B Y, Wang R R, Lin C J, Guo X, Liu B, Zhang W G. TBM penetration rate prediction based on the long short-term memory neural network. *Underground Space*, 2021, 6(6): 718–731
- Gao X J, Shi M L, Song X G, Zhang C, Zhang H W. Recurrent neural networks for real-time prediction of TBM operating parameters. *Automation in Construction*, 2019, 98: 225–235
- Li L, Liu Z B, Zhou H Y, Zhang J, Shen W Q, Shao J F. Prediction of TBM cutterhead speed and penetration rate for high-efficiency excavation of hard rock tunnel using CNN-LSTM model with construction big data. *Arabian Journal of Geosciences*, 2022, 15(3): 280
- Guo D, Li J H, Jiang S H, Li X, Chen Z Y. Intelligent assistant driving method for tunnel boring machine based on big data. *Acta Geotechnica*, 2021, 17(4): 1019–1030
- Wei M, Wang Z L, Wang X Y, Peng J L, Song Y. Prediction of TBM penetration rate based on Monte Carlo-BP neural network. *Neural Computing & Applications*, 2021, 33(2): 603–611
- Acaroglu O. Prediction of thrust and torque requirements of TBMs with fuzzy logic models. *Tunnelling and Underground Space Technology*, 2011, 26(2): 267–275
- Zhang W G, Li H R, Wu C Z, Li Y Q, Liu Z Q, Liu H L. Soft computing approach for prediction of surface settlement induced by earth pressure balance shield tunneling. *Underground Space*, 2021, 6(4): 353–363
- Chen L, Liu Z T, Mao W J, Su H Y, Lin F L. Real-time prediction of tbm driving parameters using in situ geological and operation data. *IEEE/ASME Transactions on Mechatronics*, 2022, 27(5): 4165–4176
- Zhang W G, Li H R, Li Y Q, Liu H L, Chen Y M, Ding X M. Application of deep learning algorithms in geotechnical engineering: A short critical review. *Artificial Intelligence Review*, 2021, 54(8): 5633–5673
- Farrokh E, Rostami J, Laughton C. Study of various models for estimation of penetration rate of hard rock TBMs. *Tunnelling and Underground Space Technology*, 2012, 30: 110–123
- Armaghani D J, Mohamad E T, Narayanasamy M S, Narita N, Yagiz S. Development of hybrid intelligent models for predicting TBM penetration rate in hard rock condition. *Tunnelling and Underground Space Technology*, 2017, 63: 29–43
- Armetti G, Migliazza M R, Ferrari F, Berti A, Padovese P. Geological and mechanical rock mass conditions for TBM performance prediction. The case of “La Maddalena” exploratory tunnel, Chiomonte (Italy). *Tunnelling and Underground Space Technology*, 2018, 77: 115–126
- Yang X, Gong G F, Yang H Y, Jia L H, Ying Q W. A cutterhead energy-saving technique for shield tunneling machines based on load characteristic prediction. *Journal of Zhejiang University. Science A*, 2015, 16(5): 418–426
- Xue Y D, Zhao F, Zhao H X, Li X, Diao Z X. A new method for selecting hard rock TBM tunnelling parameters using optimum energy: A case study. *Tunnelling and Underground Space Technology*, 2018, 78: 64–75
- Liu B, Wang Y X, Zhao G Z, Yang B, Wang R R, Huang D X, Xiang B. Intelligent decision method for main control parameters of tunnel boring machine based on multi-objective optimization of excavation efficiency and cost. *Tunnelling and Underground Space Technology*, 2021, 116: 104054
- Gong Q M, Zhou X X, Liu Y Q, Han B, Yin L J. Development of a real-time muck analysis system for assistant intelligence TBM tunnelling. *Tunnelling and Underground Space Technology*, 2021, 107: 103655
- Xia Y M, Yang M, Mei Y B, Ji Z Y. Influence of geological properties and operational parameters on TBM muck removal

- performance for Yinsong tunnel. *Geotechnical and Geological Engineering*, 2022, 40(4): 2291–2306
29. Khatir S, Boutchicha D, Le Thanh C, Tran-Ngoc H, Nguyen T N, Abdel-Wahab M. Improved ANN technique combined with Jaya algorithm for crack identification in plates using XIGA and experimental analysis. *Theoretical and Applied Fracture Mechanics*, 2020, 107: 102554
 30. Sharma S, Awasthi R, Sastry Y S, Budarapu P R. Physics-informed neural networks for estimating stress transfer mechanics in single lap joints. *Journal of Zhejiang University. Science A*, 2021, 22(8): 621–631
 31. Huang X, Yin X, Liu B, Ding Z W, Zhang C F, Jing B Y, Guo X S. A gray wolf optimization-based improved probabilistic neural network algorithm for surrounding rock squeezing classification in tunnel engineering. *Frontiers in Earth Science (Lausanne)*, 2022, 10: 857463
 32. Khatir S, Dekemele K, Loccufer M, Khatir T, Abdel Wahab M. Crack identification method in beam-like structures using changes in experimentally measured frequencies and Particle Swarm Optimization. *Comptes Rendus. Mécanique*, 2018, 346(2): 110–120
 33. Khatir S, Abdel Wahab M, Boutchicha D, Khatir T. Structural health monitoring using modal strain energy damage indicator coupled with teaching-learning-based optimization algorithm and isogoemetric analysis. *Journal of Sound and Vibration*, 2019, 448: 230–246
 34. Sun J, Feng B, Xu W B. Particle swarm optimization with particles having quantum behavior. In: *Proceedings of the 2004 Congress on Evolutionary Computation*. Portland: IEEE, 2004, 1: 325–331
 35. Tran-Ngoc H, Khatir S, De Roeck G, Bui-Tien T, Abdel Wahab M. An efficient artificial neural network for damage detection in bridges and beam-like structures by improving training parameters using cuckoo search algorithm. *Engineering Structures*, 2019, 199: 109637
 36. Wang Z, Wang B, Liu C, Wang W S. Improved BP neural network algorithm to wind power forecast. *Journal of Engineering (Stevenage, England)*, 2017, 2017(13): 940–943
 37. Liu Q S, Wang X Y, Huang X, Yin X. Prediction model of rock mass class using classification and regression tree integrated AdaBoost algorithm based on TBM driving data. *Tunnelling and Underground Space Technology*, 2020, 106: 103595
 38. Yin X, Liu Q S, Huang X, Pan Y C. Perception model of surrounding rock geological conditions based on TBM operational big data and combined unsupervised-supervised learning. *Tunnelling and Underground Space Technology*, 2022, 120: 104285
 39. Hou S K, Liu Y R. Early warning of tunnel collapse based on Adam-optimised long short-term memory network and TBM operation parameters. *Engineering Applications of Artificial Intelligence*, 2022, 112: 104842
 40. Teale R. The concept of specific energy in rock drilling. *International Journal of Rock Mechanics and Mining Sciences & Geomechanics Abstracts*, 1965, 2(1): 57–73
 41. Mirahmadi M, Tabaei M, Dehkordi M S. Estimation of the specific energy of TBM using the strain energy of rock mass, case study: Amir-Kabir water transferring tunnel of Iran. *Geotechnical and Geological Engineering*, 2017, 35(5): 1991–2002
 42. Liu B, Wang R, Zhao G, Guo X, Wang Y, Li J, Wang S. Prediction of rock mass parameters in the TBM tunnel based on BP neural network integrated simulated annealing algorithm. *Tunnelling and Underground Space Technology*, 2020, 95: 103103
 43. Khatir S, Abdel Wahab M. Fast simulations for solving fracture mechanics inverse problems using POD-RBF XIGA and Jaya algorithm. *Engineering Fracture Mechanics*, 2019, 205: 285–300
 44. Reinoso J, Durand P, Budarapu P R, Paggi M. Crack patterns in heterogenous rocks using a combined phase field-cohesive interface modeling approach: A numerical study. *Energies*, 2019, 12(6): 965
 45. Zhang Q L, Liu Z Y, Tan J R. Prediction of geological conditions for a tunnel boring machine using big operational data. *Automation in Construction*, 2019, 100: 73–83
 46. Hou S K, Liu Y R, Yang Q. Real-time prediction of rock mass classification based on TBM operation big data and stacking technique of ensemble learning. *Journal of Rock Mechanics and Geotechnical Engineering*, 2022, 14(1): 123–143
 47. Zhang Q, Qu C Y, Kang Y L, Huang G Y, Cai Z X, Zhao Y, Zhao H F, Su P C. Identification and optimization of energy consumption by shield tunnel machines using a combined mechanical and regression analysis. *Tunnelling and Underground Space Technology*, 2012, 28: 350–354
 48. Breiman L. Random forests. *Machine Learning*, 2001, 45(1): 5–32
 49. Zhang W G, Zhang R H, Wu C Z, Goh A T C, Wang L. Assessment of basal heave stability for braced excavations in anisotropic clay using extreme gradient boosting and random forest regression. *Underground Space*, 2022, 7(2): 233–241
 50. Cutler A, Cutler D R, Stevens J R. *Random Forests*. Ensemble Machine Learning. Boston: Springer, 2012, 157–175
 51. Refaeilzadeh P, Tang L, Liu H. Cross-validation. *Encyclopedia of Database Systems*, 2009, 5: 532–538